Available online at www.sciencedirect.com

ScienceDirect

Procedia Computer Science 4 (2011) 1343–1352

Procedia Computer Science

International Conference on Computational Science, ICCS 2011

An overlapping domain decomposition method for a polymer exchange membrane fuel cell model

Mingyan He[a], Ziping Huang[a,b], Cheng Wang[a,*], Pengtao Sun[c], Shuang Zhai[d]

[a] *Department of Mathematics, Tongji University, Shanghai, 200092, P.R. China*
[b] *Chinese-German College, Tongji University, Shanghai, 200092, P.R. China*
[c] *Department of Mathematical Sciences, University of Nevada Las Vegas, 4505 Maryland Parkway, Las Vegas, NV 89154, USA*
[d] *School of Automotive Engineering, Tongji University, Shanghai, 200092, P.R. China*

Abstract

The structure of channels, cell material and operation parameters are usually implemented in different ways from anode to cathode in the actual work to seek better performance for polymer exchange membrane fuel cell (PEMFC). However, the asymmetrical structure of such specific design often leads to non-matching grids in the numerical simulation of PEMFC, especially when the structured grids are used. Besides, different mesh sizes are often used in the simulation for anode and cathode in order to obtain both high accuracy and relatively low computational cost. In this paper, an overlapping domain decomposition finite element method is studied to deal with the non-matching grids for a simplified two-dimensional single-phase PEMFC model. Numerical experiments demonstrate that our methods are able to deal with PEMFC simulation on the non-matching grids with fast convergence and low mass balance error.

Keywords: PEMFC, non-matching grids, overlapping domain decomposition, numerical simulation

1. Introduction

Polymer exchange membrane fuel cells (PEMFCs) have been used in a large number of industries worldwide because of their advantages such as low environmental impact, rapid start-up and high power density. Through tremendous progress has been made in the past decade, industries are currently placing their focus on fuel cell design and engineering for better performance, improved durability, cost reduction and better cold-start characteristics. This new focus has led to an urgent need for identification, understanding, prediction, control and optimization of various transport and electrochemical processes that occur on disparate length scales in fuel cells [1, 2, 3, 4].

The performance of fuel cell is affected by many factors, such as material parameters, operating conditions, different channel structures and so on. Berning and Djilali [5] investigated the effect of various operational parameters such as the temperature and pressure on the fuel cell performance in detail. Combining the modeling with experiments, L. Wang [6] studied the effect of different fuel cell operating temperatures, cathode and anode humidi1ities, operating pressures and various combinations of these parameters on the performance of PEMFC. The various influences of the

*Corresponding author
Email addresses: hemingyan1985@yahoo.com.cn (Mingyan He), huangziping@tongji.edu.cn (Ziping Huang), wangcheng@tongji.edu.cn (Cheng Wang), pengtao.sun@unlv.edu (Pengtao Sun), playerzhaishuang@yahoo.cn (Shuang Zhai)

Selection and/or peer-review under responsibility of Prof. Mitsuhisa Sato and Prof. Satoshi Matsuoka
doi:10.1016/j.procs.2011.04.145

straight, interdigitated and serpentine gas flow channels have been studied in [7, 8, 9]. Shimpalee [10] investigated how the serpentine flow fields with different channel sizes can affect cell performance and species distributions for both automotive and stationary conditions. Besides, a single-path serpentine flow-field design was used for studying the effect of channel dimensions, including different channel width, land width and channel depth, on the hydrogen consumption at the anode [11]. Cheng [12] found that the flow channel size also affects the reactant transport in a PEMFC stack. Thus the size and shape of the channel play a key role in the design of PEMFC.

For better performance, therefore, different structures for the anode and cathode gas channels are used in PEMFC practical design. This asymmetrical structure can keep the balance of pressures on both sides of the membrane. Thus the water management in cathode can be improved and the duration of fuel cell can be prolonged. However, the asymmetrical structure often leads to non-matching grids in numerical simulations when partitioning with structured grids such as hexahedra. That is to say, because different grid generation methods are used in anode and cathode due to the asymmetric structure, the grids on both sides of membrane are not matched, which produces great challenges in numerical simulation. On the other hand, since oxygen reduction reaction occurs in cathode, the variation of physical quantities such as water concentration are more significant in cathode than in anode. For example, a possible cathode flooding may occur and show a gradual decrease in cell performance. Also, the increased water content of membrane in equilibrium with liquid water in turn results in more water molecules being dragged electro-osmotically to the cathode GDL thus leading to severe cathode flooding. So it is necessary for cathode to simulate these phenomena accurately by a refined grid. On all accounts, a new discretization scheme is thus needed for an asymmetric PEMFC structure with a non-matching grid.

Though an unstructured grid partitioned by tetrahedra or triangles can be used for this asymmetrical fuel cell in one-domain approach, structured grids such as hexahedron and quadrilateral, not only easily implemented, but also have super convergence [13, 14, 15]. So an overlapping domain decomposition method (DDM) is worthy of being studied to deal with the non-matching structured grids arising from multiple asymmetric subdivisions. The objective of this paper is to study a specific domain decomposition discretization scheme for a two-dimensional single-phase transport model of PEMFC. To do so, we firstly introduce a 2D simplified steady-state transport model in this paper.

The rest of this paper is organized as follows. Governing equations for single-phase steady-state transport problem are defined in Section 2. In Section 3, we introduce the method of the combined finite element-upwind finite volume and an overlapping domain decomposition method, then a new discretization scheme is designed to deal with the non-matching grids. Numerical simulations of several practical cases are illustrated in Section 4, indicating that our numerical schemes significantly improve the computational performance in the senses of efficiency and accuracy in contrast to an unstructured grid on the same asymmetric PEMFC.

2. The 2D steady-state transport model

Based on [1, 16], a fundamental fuel cell model consists of five principles of conservation: mass, momentum, species, charge, and thermal energy. Typically the fuel cell is divided into seven subregions: the anode gas channel, anode gas diffusion layer (GDL), anode catalyst layer (CL), ionomeric membrane, cathode gas channel, cathode GDL, and cathode CL. In the following we specifically focus our interests on mass, momentum conservation and water concentration arising in all seven subregions.

2.1. Governing equations

Flow equations. For flow field with velocity $\vec{u}$ and pressure P as unknowns, we have the following modified Navier-Stokes equations [1]

$$\nabla \cdot (\rho \vec{u}) = 0, \tag{1}$$

$$\frac{1}{\varepsilon^2} \nabla \cdot (\rho \vec{u} \vec{u}) = -\nabla P + \nabla \cdot (\mu \nabla \vec{u}) + S_u, \tag{2}$$

where ε is porosity, namely, volume fraction of gases phase in porous region, ρ is density, μ is effective viscosity. We know (1) is an exact continuity equation, and (2) represents a modified momentum equation, in which we indicate that the additional source term S_u is named as Darcy's drag and defined as follows

$$S_u = -\frac{\mu}{K} \vec{u}, \tag{3}$$

Table 1: Physical coefficients and parameters

Parameter	Symbol	Value	Unit
Anode/cathode gas channel width	δ_{CH}	3.180	mm
Anode/cathode GDL width	δ_{GDL}	0.235	mm
Anode/cathode CL width	δ_{CL}	0.010	mm
Membrane width	δ_{mem}	0.018	mm
Cell length	l_{cell}	70	mm
Water vapor diffusivity	D_{gas}	2.6×10^{-5}	m^2/s
Porosity of GDL and CL	ε	0.6	
Porosity of membrane	ε	0.26	
Effective viscosity	μ	3.1664×10^{-5}	$kg/m/s$
Vapor density	ρ	0.882	kg/m^3
Electro-osmotic drag coefficient	n_d	1.5	
Transfer current density at the left end	j_1	20000	A/m^2
Transfer current density at the right end	j_2	10000	A/m^2

where K is hydraulic permeability, where K is hydraulic permeability(m^2), defined as

$$K = \begin{cases} 2 \times 10^{-12} & \text{GDL, CL} \\ \infty & \text{gas channel.} \end{cases} \tag{4}$$

The definition of K implies that gas channel is considered as completely permeable, while GDL and CL are presented as porous media with small permeability.

Species concentration equation. Water management is critical to achieve high performance for PEMFC. Therefore, without loss of generality, in order to focus on water management topics, we typically consider water as the only component in the following simplified species concentration equation. In this paper we only consider a single-phase model for water concentration equation. The single-phase model described herein considers the total water amount without distinguishing liquid water from water vapor. This approach is valid under the condition that liquid saturation within the GDL is low. This approach is particularly well suited for fuel cell simulations under low humidity operation, a major application of single-phase models.

Water concentration equation in single gaseous phase is defined as follows with respect to concentration C [1]

$$\nabla \cdot (\vec{u}C) = \nabla(D_g^{eff} \nabla C) + S_{H_2O}, \tag{5}$$

where $D_g^{eff} = \varepsilon^{1.5} D_{gas}$ is the effective water vapor diffusivity, namely, the constant diffusivity in gaseous water region. The source term S_{H_2O} is given as follows.

$$S_{H_2O} = \begin{cases} -\nabla \cdot (\frac{n_d}{F} \vec{i}_e) - \frac{j}{2F} & \text{in cathode CL} \\ -\nabla \cdot (\frac{n_d}{F} \vec{i}_e) & \text{in anode CL} \\ 0 & \text{otherwise,} \end{cases} \tag{6}$$

where n_d, the electro-osmotic drag coefficient, is a constant value in our simulation. $\nabla \cdot \vec{i}_e = -j$ which is derived from the continuity equation of proton potential. $\vec{i}_e$ is the current density vector and j is the volumetric transfer current of the reaction (or transfer current density) defined by a linear function as follows

$$j = j_1 - (j_1 - j_2)\frac{x}{l_{cell}}, \tag{7}$$

where j_1, j_2, are technically given in Table 1. (7) is the linear simplification of Butler-Volmer equation, indicating that the transfer current density linearly decreases from a constant local current density j_1, at the left end of membrane/cathode interface (top wall) to another constant local current density j_2 at the right end. This is an approximation of transfer current density for our simplified single-phase PEMFC model due to the absence of proton and electron potentials[17].

2.2. Computational domain and boundary conditions

The computational domain is schematically shown in Fig.1. The horizontal x-axis represents the flow direction and the vertical y-axis points in the through-plane direction. The geometric sizes of this computational domain are marked in Fig. 1 as well.

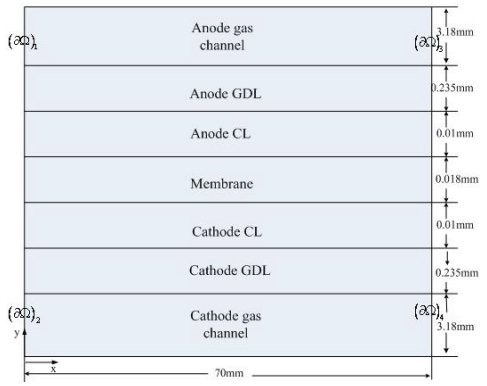

Figure 1: Domain

At the inlet of the gas channel ($(\partial\Omega)_1, (\partial\Omega)_2$ in Fig. 1), flow rate is defined as a parabolic-like function, water concentration are specified as a constant. At the outlet ($(\partial\Omega)_3, (\partial\Omega)_4$ in Fig. 1), both velocity and concentration fields are assumed to be fully developed. Hence, based on this computational domain, the boundary conditions are indicated as follows.

For flow field equation (1) and (2), the following boundary conditions hold with respect to velocity $\vec{u} = (u_1, u_2)$:

$$u_1 = u_1|_{inlet},\ u_2 = 0 \quad \text{on } (\partial\Omega)_1, (\partial\Omega)_2, \tag{8}$$

$$(PI - \mu\nabla\vec{u}) \cdot \vec{n} = 0 \quad \text{on } (\partial\Omega)_3, (\partial\Omega)_4, \tag{9}$$

$$u_1 = 0,\ \ u_2 = 0 \qquad \text{otherwise}, \tag{10}$$

where $u_1|_{inlet}$, defined as a parabolic-like function, is given in (26). And $\vec{u} = 0$, $P = 0$ in membrane because no flow field exists there.

For water concentration (5), the following boundary conditions hold with respect to concentration C:

$$C = C_{in} \quad \text{on } (\partial\Omega)_1, (\partial\Omega)_2, \tag{11}$$

$$\frac{\partial C}{\partial n} = 0 \quad \text{otherwise.} \tag{12}$$

Governing equations (1), (2) and (5), together with the definitions of physical coefficients and parameters in Table 1 and the boundary conditions above, constitute a simplified 2D steady-state single-phase transport model of polymer exchange membrane fuel cell.

3. Numerical simulation methods

3.1. Domain decomposition

To study effective numerical methods for non-matching grids arising from the simulation of PEMFC, first of all, we split the domain (Ω), shown in Fig.1, to two overlapping subdomains: one is the anode and membrane (Ω_a), another is the cathode and membrane (Ω_c). The interface between anode CL and membrane is denoted as Γ_a, and the interface between cathode CL and membrane is denoted as Γ_c. The classical overlapping Schwarz alternating method[18] is used in these two subdomains. Thus we are able to reformulate equations (1), (2) and (5) to two Dirichlet-type interfacial boundary value subproblems.

$$\text{(Problem A)}\begin{cases} \nabla\cdot(\rho\vec{u}_a)=0 & \text{in } \Omega_a \\ \frac{1}{\varepsilon^2}\nabla\cdot(\rho\vec{u}_a\vec{u}_a)=-\nabla P_a+\nabla\cdot(\mu\nabla\vec{u}_a)-\frac{\mu}{K}\vec{u}_a & \text{in } \Omega_a \\ \nabla\cdot(\vec{u}_aC_a)=\nabla(D_g^{eff}\nabla C_a)+S_{H_2O} & \text{in } \Omega_a \\ u_{1,a}=u_{1,a}|_{inlet}, u_{2,a}=0, C_a=C_{a,in} & \text{on } (\partial\Omega)_1 \\ (P_aI-\mu\nabla\vec{u}_a)\cdot\vec{n}=0 & \text{on } (\partial\Omega)_3 \\ C_a=C_c & \text{on } \Gamma_c \\ u_{1,a}=u_{2,a}=0, \frac{\partial C}{\partial n}=0 & \text{on other boundaries.} \end{cases} \tag{13}$$

$$\text{(Problem C)}\begin{cases} \nabla\cdot(\rho\vec{u}_c)=0 & \text{in } \Omega_c \\ \frac{1}{\varepsilon^2}\nabla\cdot(\rho\vec{u}_c\vec{u}_c)=-\nabla P_c+\nabla\cdot(\mu\nabla\vec{u}_c)-\frac{\mu}{K}\vec{u}_c & \text{in } \Omega_c \\ \nabla\cdot(\vec{u}_cC_c)=\nabla(D_g^{eff}\nabla C_c)+S_{H_2O} & \text{in } \Omega_c \\ u_{1,c}=u_{1,c}|_{inlet}, u_{2,c}=0, C_c=C_{c,in} & \text{on } (\partial\Omega)_2 \\ (P_cI-\mu\nabla\vec{u}_c)\cdot\vec{n}=0 & \text{on } (\partial\Omega)_4 \\ C_c=C_a & \text{on } \Gamma_a \\ u_{1,c}=u_{2,c}=0, \frac{\partial C}{\partial n}=0 & \text{on other boundaries.} \end{cases} \tag{14}$$

Since $\vec{u}=0$ in membrane, there is no degree of freedom in our numerical simulation for Problem A and Problem C. The definitions of subproblems Problem A and Problem C imply that we need to solve these two subproblems iteratively by a given initial guess $\vec{u}_a^0$ and $\vec{u}_c^0$.

3.2. Weak forms

Considering various nonlinearities of equations, we particularly employ Picard's scheme to linearize the nonlinear source term in Problem A. With given $\vec{u}_a^k$ from the kth step, find $(\vec{u}_a^{k+1}, P_a^{k+1})$ such that for $k=0,1,2...$

$$\frac{1}{\varepsilon^2}\nabla\cdot(\rho\vec{u}_a^k\vec{u}_a^{k+1})=\nabla\cdot(\mu\nabla\vec{u}_a^{k+1})-\nabla P_a^{k+1}-\frac{\mu}{K}\vec{u}_a^{k+1}, \tag{15}$$

$$\nabla\cdot\vec{u}_a^{k+1}=0. \tag{16}$$

In subdomain Ω_a we define

$$\begin{aligned} V_a &:= \{\vec{v}_a=(v_{1,a},v_{2,a})^\top\in[H^1]^2 \mid v_{1,a}|_{(\partial\Omega)_1}=u_{1,a}|_{inlet}, v_{2,a}|_{(\partial\Omega)}=0\},\\ Q_a &:= \{w\in H^1 \mid w|(\partial\Omega)_1=C_{in,a}\},\\ P_a &:= L^2(\Omega_a),\\ \widetilde{V}_a &:= \{\vec{v}_a=(v_{1,a},v_{2,a})^\top\in[H^1]^2 \mid v_{1,a}|_{(\partial\Omega)_1}=0, v_{2,a}|_{(\partial\Omega)}=0\},\\ \widetilde{Q}_a &:= \{w\in H^1 \mid w|(\partial\Omega)_1=0\}. \end{aligned}$$

Then for any $(\vec{v}_a, q_a, W_a)\in\widetilde{V}_a\times P_a\times\widetilde{Q}_a$, find $(\vec{u}_a^{k+1}, P_a^{k+1}, C_a^{k+1})\in V_a\times P_a\times Q_a$, such that

$$\begin{cases} (\mu\nabla\vec{u}_a^{k+1},\nabla\vec{v}_a)+(\frac{\rho}{\varepsilon^2}\nabla\vec{u}_a^k\vec{u}_a^{k+1},\vec{v}_a)-(P_a^{k+1},\nabla\vec{v}_a)+(\frac{\mu}{K}\vec{u}_a^{k+1},\vec{v}_a)=0 \\ (\nabla\vec{u}_a^{k+1},q_a)=0 \\ (D_g^{eff}\nabla C_a^{k+1},\nabla w_a)-((\vec{u}_a^kC_a^{k+1}),\nabla w_a)+\int_{(\partial\Omega)_3}\vec{u}_a^k\cdot\vec{n}C_a^{k+1}w_a dy=(S_{H_2O},w_a). \end{cases} \tag{17}$$

Similarly, in subdomain Ω_c we define

$$\begin{aligned} V_c &:= \{\vec{v}_c=(v_{1,c},v_{2,c})^\top\in[H^1]^2 \mid v_{1,c}|_{(\partial\Omega)_2}=u_{1,c}|_{inlet}, v_{2,c}|_{(\partial\Omega)_2}=0\},\\ Q_c &:= \{w\in H^1 \mid w|(\partial\Omega)_2=C_{in,c}\},\\ P_c &:= L^2(\Omega_c),\\ \widetilde{V}_c &:= \{\vec{v}_c=(v_{1,c},v_{2,c})^\top\in[H^1]^2 \mid v_{1,c}|_{(\partial\Omega)_2}=0, v_{2,c}|_{(\partial\Omega)_2}=0\},\\ \widetilde{Q}_c &:= \{w\in H^1 \mid w|(\partial\Omega)_2=0\}. \end{aligned}$$

Then for any $(\vec{v}_c, q_c, w_c) \in \widetilde{V}_c \times P_c \times \widetilde{Q}_c$, find $(\vec{u}_c^{k+1}, P_c^{k+1}, C_c^{k+1}) \in V_c \times P_c \times Q_c$, such that

$$\begin{cases} (\mu\nabla\vec{u}_c^{k+1}, \nabla\vec{v}_c) + (\frac{\rho}{\varepsilon^2}\nabla\vec{u}_c^{k}\vec{u}_c^{k+1}, \vec{v}_c) - (P_c^{k+1}, \nabla\vec{v}_c) + (\frac{\mu}{K}\vec{u}_c^{k+1}, \vec{v}_c) = 0 \\ (\nabla\vec{u}_c^{k+1}, q_c) = 0 \\ (D_g^{eff}\nabla C_c^{k+1}, \nabla w_c) - ((\vec{u}_c^{k}C_c^{k+1}), \nabla w_c) + \int_{(\partial\Omega)_4} \vec{u}_c^{k} \cdot \vec{n} C_c^{k+1} w_c dy = (S_{H_2O}, w_c). \end{cases} \tag{18}$$

3.3. Discretization schemes

In correspondence with weak forms (17) and (18), we design the combined finite element-upwind finite volume discretization schemes for the flow equations (1) and (2), and apply the finite element method to the water concentration equation (5). Note that the convection term $(\frac{\rho}{\varepsilon^2}\nabla\vec{u}^{k}\vec{u}^{k+1}, \vec{v})$ may dominant due to the large velocity $\vec{u}$. Therefore, in order to stabilize the numerical computation for nonlinear iteration (15), we employ the upwind finite volume method to overcome the possibly dominant convection term [17, 19, 20, 21, 22, 23].

Since finite-difference based upwind scheme cannot directly work for finite element discretization, as substitutes, streamline-diffusion scheme [17, 24, 25, 26, 27] is appropriately chosen to deal with dominant convectional coefficients in the framework of finite element method. Typically, we apply streamline-diffusion scheme to concentration equation (5), due to the specific convective features.

First we define a partition $\mathcal{T}_{h_i}$ with the maximum mesh size h_i in Ω_i (i, j represent a or c), and $\Sigma_{i,j}$ is the set of mesh points of $\mathcal{T}_{h_i}$ on Γ_j. Let $(\cdot,\cdot)_{\Omega_i}$ stand for the L^2 inner product in Ω_i.

To discretize weak form (17) and (18), we introduce the finite element space $S_{h_i} = V_{h_i} \times P_{h_i} \times Q_{h_i} \subset V_i \times P_i \times Q_i$ on $\mathcal{T}_{h_i}$, where V_{h_i}, $P_{h_i}$and Q_{h_i} are the piecewise bilinear finite element space. Especially for Q_{h_i}, we have

$$Q_{h_a} := \{w \in H^1(\Omega_a) \mid w|_{\Gamma_c} = f_a\}, \tag{19}$$

$$Q_{h_c} := \{w \in H^1(\Omega_c) \mid w|_{\Gamma_a} = f_c\}, \tag{20}$$

where f_a and f_c represent the values of points in the sets of $\Sigma_{a,c}$ and $\Sigma_{c,a}$, respectively, which are obtained by the previous alternating step values of points $\Sigma_{c,c}$ and $\Sigma_{a,a}$by lagrange interpolation.

For flow equations, we introduce the following combined finite element-upwind finite volume schemes [23].

For any given $(\vec{v}, q) \in \widetilde{V}_{h_i} \times P_{h_i}$, find $(\vec{u}_{h_i}^{k+1}, P_{h_i}^{k+1}) \in V_{h_i} \times P_{h_i} (k = 0, 1, 2, ...)$, such that

$$\begin{cases} (\mu\nabla\vec{u}_{h_i}^{k+1}, \nabla\vec{v})_{\Omega_{i,h_i}} - (P_{h_i}^{k+1}, \nabla\vec{v})_{\Omega_{i,h_i}} + (\frac{\mu}{K}\vec{u}_{h_i}^{k+1}, \vec{v})_{\Omega_{i,h_i}} + \sum_{i=1}^{N} v_i \sum_{P_j \in \partial A_i} \frac{\rho}{\varepsilon^2} \int_{\Gamma_{ij}} (\vec{u}_{h_i}^{k} \cdot \vec{n}) ds((r_{ij} - 1)(\vec{u}_i^{k+1} - \vec{u}_j^{k+1})) = 0 \\ (\nabla\vec{u}_{h_i}^{k+1}, q)_{\Omega_{i,h_i}} = 0. \end{cases} \tag{21}$$

For water concentration equation, in anode, for any given $w_a \in \widetilde{Q}_{h_a}$, find $C_{h_a}^{k+1} \in Q_{h_a}$, such that

$$D_g^{eff}(\nabla C_{h_a}^{k+1}, \nabla w_a) - (\vec{u}_{h_a} C_{h_a}^{k+1}, \nabla w_a) + \int_{(\partial\Omega)_3} \vec{u}_a^{k} \cdot \vec{n} C_a^{k+1} w_a dy + \delta_{sld}(h_a)(\vec{u}_{h_a} \cdot \nabla C_{h_a}^{k+1}, \vec{u}_{h_a} \cdot \nabla w_a) = (S_{H_2O}, w_a). \tag{22}$$

In cathode, for any given $w_c \in \widetilde{Q}_{h_c}$, find $C_{h_c}^{k+1} \in Q_{h_c}$, such that

$$D_g^{eff}(\nabla C_{h_c}^{k+1}, \nabla w_c) - (\vec{u}_{h_c} C_{h_c}^{k+1}, \nabla w_c) + \int_{(\partial\Omega)_4} \vec{u}_c^{k} \cdot \vec{n} C_c^{k+1} w_c dy + \delta_{sld}(h_c)(\vec{u}_{h_c} \cdot \nabla C_{h_c}^{k+1}, \vec{u}_{h_c} \cdot \nabla w_c) = (S_{H_2O}, w_c), \tag{23}$$

where the last term in the left hand side of (22) and (23) is a stabilizing term, derived from streamline-diffusion scheme. Basically we hold $\delta_{sld}(h) = C_{sld}h$, C_{sld} is a certain constant parameter, which is chosen artificially with least possible on the premise of optimal stability. Therefore, when mesh size h is sufficiently small, the additional diffusive terms eventually approximate to zero with the rate of convergence $O(h)$. So numerical discretization (22) and (23) still approache the original one when h is small enough [17].

3.4. Numerical algorithm

Now, we are in position to describe the overlapping domain decomposition algorithm with the finite element discretizations (21)-(23).

Algorithm: Given $\vec{u}_h^0, C_h^0$, the following procedures are successively executed ($k > 0$):

Step 1. Solve (21) and (**??**) in Ω_a and Ω_c for $(\vec{u}_{h_i}^{k+1}, P_{h_i}^{k+1})$, respectively, until

$$\|\vec{u}_{h_i}^{k+1} - \vec{u}_{h_i}^{k}\|_{L^2(\Omega_i)} + \|P_{h_i}^{k+1} - P_{h_i}^{k}\|_{L^2(\Omega_i)} < \text{tolerance}. \tag{24}$$

Step 2. Solve (22) for $C_{h_a}^{k+1}$, and construct the finite element space $\widetilde{Q}_{h_c}$ for Ω_c.

Step 3. Solve (23) for $C_{h_c}^{k+1}$, and construct the finite element space $\widetilde{Q}_{h_a}$ for Ω_a.

Step 4. Compute the following stopping criteria:

$$\|C_{h_a}^{k+1} - C_{h_a}^{k}\|_{L^2(\Gamma_c)} + \|C_{h_c}^{k+1} - C_{h_c}^{k}\|_{L^2(\Gamma_a)} < \text{tolerance}, \tag{25}$$

which is the relative convergence error in two successive iteration steps on the interfaces of CLs and membrane.

If yes, then numerical computation is complete. Otherwise, go back to the step 2 and continue.

It is well known that the flow profile is parabolic under steady flow conditions once laminar flow is fully developed in long and straight channel. Based on this fact, in the following numerical experiments, we assign the Dirichlet boundary condition of velocity at the inlet as follows

$$u_1|_{inlet} = \begin{cases} u_{in,c}\sin(y\pi/\delta_{CH}) & \text{at cathode inlet } (\partial\Omega)_2 \\ u_{in,a}\sin((y - 3.688\times 10^{-3})\pi/\delta_{CH}) & \text{at anode inlet } (\partial\Omega)_1 \end{cases} \quad 0 \le y \le \delta_{CH}, \tag{26}$$

where $3.688\times10^{-3} = \delta_{CH}+\delta_{GDL}+\delta_{CL}+\delta_{mem}$. Since the Schwarz alternating method does not depend on the dimension of the spatial domain but only the water concentration variable, we can directly generalize it to the three-dimensional situation. Consequently numerical discretizations (21)-(23) are readily extendable to a three-dimensional PEMFC model without any difficulty.

4. Numerical results

In this section, we will carry out the following two numerical experiments which indicate that our methods are effective to deal with the non-matching grids, see Fig.2 for example, in the simulation of the PEMFC.

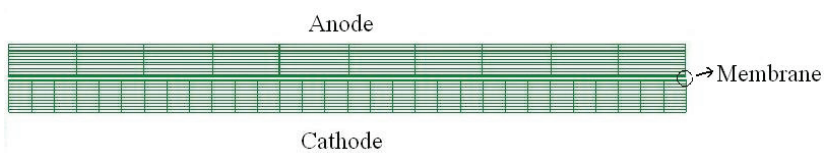

Figure 2: An example of non-matching grids

Case 1: $u_{in,a} = 5\ m/s, u_{in,c} = 3\ m/s, C_{in,a} = 12\ mol/m^3, C_{in,c} = 4\ mol/m^3$**.** Provided that a practical boundary condition $u_{in} = 5\ m/s, C_{in} = 12\ mol/m^3$ at the inlet of anode and $u_{in} = 3\ m/s, C_{in} = 4\ mol/m^3$ at the inlet of cathode, we gain reasonable physical solutions by employing numerical discretization (21)-(23).

First of all, we define a rectangular partition $\mathcal{T}_h$ on the domain with 10 intervals along x-direction for the length of the anode, 30 intervals for that of the cathode and 40, 40, 16, 16 intervals along y-direction for the width of gas channel, GDL, CL and membrane, respectively. So the number of total grids in anode and cathode are $10\times(40+40+16+16) = 1120$ and $30\times(40+40+16+16) = 3360$, separately (mesh3 in Table 2). The tolerance of our stopping criteria (25) for Schwarz alternating iteration is 10^{-20}. The Fig.3 displays the convergence history of water concentration with the numbers of the iteration in our overlapping domain decomposition algorithm.

In order to verify the correctness of our numerical solutions, we compute the relative error of mass balance in terms of the numerical fluxes at the inlet and outlet.

Table 2: Convergent mass balance error for Case 1 with different grids

	Nodes	DDM with quadrangle grids		Unstructured triangulation grids	
		Grids	Error	Grids	Error
Mesh1	1218	280+840	1.0416e-3	2260	5.5143e-3
Mesh2	2394	560+1680	6.6184e-4	4678	1.9566e-3
Mesh3	4746	1120+3360	5.2243e-4	9404	8.8962e-4
Mesh4	9450	2240+6720	4.5789e-4	19492	6.2022e-4

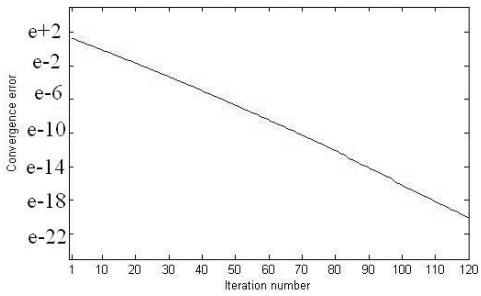

Figure 3: Convergence history of concentration by DDM

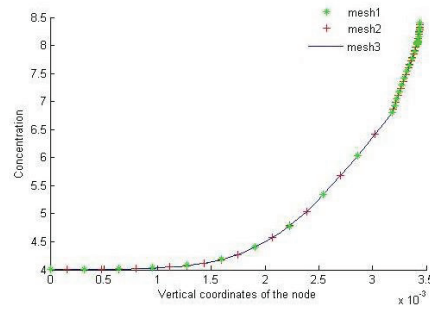

Figure 4: Comparison of mesh1, 2 and 3

$$\text{mass balance error} = \frac{|\int_{(\partial\Omega)_{outlet}} C u_1 d\tau - \int_{(\partial\Omega)_{inlet}} C_{in} u_1|_{inlet} d\tau - \int_{\Omega} S_{H_2O} dS|}{\int_{(\partial\Omega)_{inlet}} C_{in} u_1|_{inlet} d\tau} \tag{27}$$

By plugging the assigned and the computed concentration C as well as horizontal velocity u_1 in equation (27), we attain a convergent mass balance error for our numerical solutions along with the continuously refining grids, as shown in Table 2. We see that, at current mesh density (mesh3), an more accurate mass balance error is attained for the gained numerical solutions. And our method with quadrangle grids have lower convergence error than unstructured triangulation grids. Fig.4 displays the concentration of water in cathode on grid line where $y = 35\ mm$ for three different meshes in Table 2. We see that the concentration of water converges as the mesh size tends to zero. Water vapor is generated in cathode catalyst layer by the reaction and gas diffusion is the dominant transport mechanism in porous media. So the water concentration has a gradient change in the vertical direction.

In the following, the focus is placed on elucidating numerical results shown in Figs. 5-8.

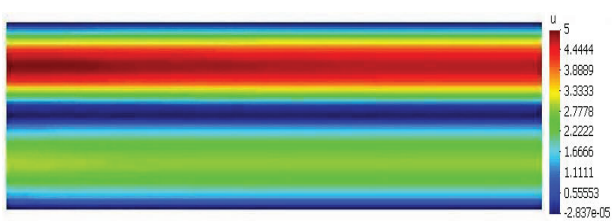

Figure 5: Horizontal velocity produced by DDM

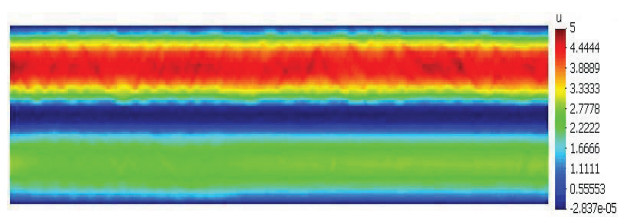

Figure 6: Horizontal velocity with unstructured grids

The Fig.5 and Fig.7 show the velocity field in anode and cathode of fuel cell produced by the overlapping domain decomposition method. As expected, there is a large difference in the velocity scale between the porous media and the open channel. The velocity in porous GDL is at least two orders of magnitude smaller than that in the open gas channel, indicating that gas diffusion is the dominant transport mechanism in porous GDL. Porous CL has a smaller velocity than GDL due to the inferior diffusion ability. Fig.6 shows the horizontal velocity produced by unstructured triangulation grids with the same number of nodes, from which we can see that the distribution of the velocity is not smooth enough compared to Fig.5, indicating that an unstructured coarse grid cannot produce a comparably more

accurate solution than a structured grid with the same number of nodes. Note that a relatively coarse grid with better numerical solutions is always promising in the simulation of a real-time problem.

Fig.8 displays the water concentration distribution, presenting in the phase of water vapor, in anode and cathode. As shown in this figure, significant variations are displayed in both anode and cathode; in the porous media there is an increased water vapor concentration along the channel.

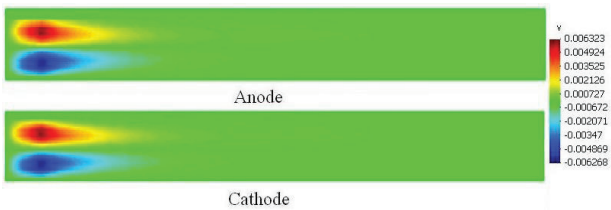

Figure 7: Vertical velocity produced by DDM

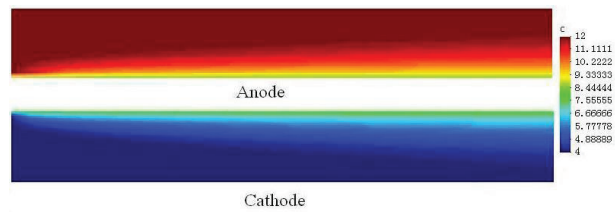

Figure 8: Water concentration produced by DDM

Case 2: $u_{in,a} = 20\ m/s, u_{in,c} = 3\ m/s, C_{in,a} = 12\ mol/m^3, C_{in,c} = 4\ mol/m^3$**.** In Case 1, a small difference between the inlets of anode and cathode does not make visible difference for the vertical velocities. In this case, we keep the same water concentration at the inlets of anode and cathode with Case 1, and let the velocity at the inlet of anode increasing dramatically, which means that the difference between $u_{in,a}$ and $u_{in,c}$ is enlarged. Fig.9 shows the distribution of vertical velocity in anode and cathode. As the air flows down the channel, the values of vertical velocity is higher in anode than that in cathode. We also attain a relatively accurate mass balance error for the numerical solutions in this case, as shown in Table 3.

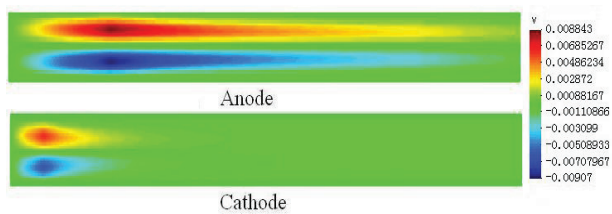

Figure 9: Distributions of vertical velocities in Case 2

Table 3: Convergent mass balance error for Case 2

Outlet flux	F_{out}	5.099944e-1
Inlet flux	F_{in}	5.098993e-1
Source	S	-3.752656e-006
Mass balance error	$\frac{\lvert F_{out} - F_{in} - S \rvert}{F_{in}}$	1.9376e-004

5. Conclusions and future work

In this paper, a simplified single-phase 2D steady PEMFC model is introduced by a modified Navier-Stokes equations for mass and momentum, and a conservation equation for water concentration. Because there are some specific structure designs for PEMFC requiring different channel structures for anode and cathode, a structured quadrilateral mesh on such PEMFC shall lead to a non-matching grid, where the grids are not matched in MEA. In the future work, the relatively abundant water accumulation effect at the cathode due to the coupling of two-phase transport in GDL with other interdisciplinary issues such as oxygen reduction reaction and electro-osmotic drag also requires a more precise simulation for water equation on a finer grid at the cathode than that at the anode. Based on the combined

finite element-upwind finite volume methods and the overlapping domain decomposition method, a new discretization scheme is designed and implemented for this specific PEMFC model. Numerical experiments demonstrate that our methods are able to deal with the non-matching grids with fast convergence and obtain a relatively accurate numerical solution with low mass balance error. The derived discretization scheme will be also studied for two-phase unsteady and/or fuel cell stack model in our further work.

Acknowledgments

The authors acknowledge ”Applied Mathematics Chair Fund of China-German College” (0900101021). Pengtao Sun is supported in part by NSF Grant DMS-0913757 and Chinese 111-Program for energy-saving and environment friendly automobile (B08019).

Reference

[1] C.-Y. Wang, Fundamental models for fuel cell engineering, Journal of the Electrochemical Society 104 (2004) 4727–4766.
[2] U. D. of Energy, O. of Fossil Energy, Fuel cell handbook(seventh edition), EG and G Technical Services.Int, West Virginia, 2004.
[3] C. Y. Wang, S. Um, K. Chen, Computational fluid dynamics modeling of proton exchange membrane fuel cells, Journal of the Electrochemical Society 147 (2000) 4485–4493.
[4] Y. Wang, C.-Y. Wang, Dynamics of polymer electrolyte fuel cells undergoing load changes, Electrochimica Acta 51 (2006) 3924–3933.
[5] T. Berning, N. Djilali, Three-dimensional computational analysis of transport phenomena in a PEM fuel cellła parametric study, Journal of Power Sources 124 (2003) 440–452.
[6] L. Wang, A. Husar, T. Zhou, H. Liu, A parametric study of PEM fuel cell performances, International Journal of Hydrogen Energy 28 (2003) 1263–1272.
[7] S. Um, C.Y.Wang, Three-dimensional analysis of transport and electrochemical reaction in polymer electrolyte fuel cells, Journal of Power Sources 124 (2004) 40–51.
[8] G. Hu, J. Fan, S. Chen, Y. Liu, K. Cen, Three-dimensional numerical analysis of proton exchange membrane fuel cells (PEMFCs) with conventional and interdigitated flow fields, Journal of Power Sources 136 (2004) 1–9.
[9] P. T. Nguyen, T. Berning1, N. Djilali, Computational model of a PEM fuel cell with serpentine gas flow channels, Journal of Power Sources 130 (2004) 149–157.
[10] S. Shimpalee, J. V. Zee, Numerical studies on rib and channel dimension of flow-field on PEMFC performance, International Journal of Hydrogen Energy 32 (2007) 842–856.
[11] A. Kumar, R. G. Reddy, Effect of channel dimensions and shape in the flow-field distributor on the performance of polymer electrolyte membrane fuel cells, Journal of Power Sources 113 (2003) 11–18.
[12] C.-H. Cheng, H.-H. Linb, Numerical analysis of effects of flow channel size on reactant transport in a proton exchange membrane fuel cell stack, Journal of Power Sources 194 (2009) 349–359.
[13] L. B. Wahlbin, Superconvergence in Galerkin Finite Element Methods, Springer-Verlag, Berlin, 1995.
[14] R. E. Bank, J. Xu, Asymptotically exact a posteriori error estimators, part I: grids with superconvergence, SIAM Journal on Numerical Analysis 41 (2003) 2294–2312.
[15] Y. Q. Huang, J. Xu, Superconvergence for quadratic triangular finite elements on mildly structured grids, Mathematics of computation 77 (2008) 1253–1268.
[16] H. Ju, H. Meng, C.-Y. Wang, A single-phase, non-isothermal model for pem fuel cells, International Journal of Heat and Mass Transfer 48 (2005) 1303–1315.
[17] P. Sun, G. Xue, C. Wang, J. Xu, Fast numerical simulation of two-phase transport model in the cathode of a polymer electrolyte fuel cell, Communications in Computational Physics 6 (2009) 49–71.
[18] A. Toselli, O. B.Widlund, Domain decomposition methods - algorithms and theory, Springer, New York, 2005.
[19] D. Kroner, M. Rokyta, Convergence of upwind finite volume schemes for scalar conservation laws in two dimensions, SIAM Journal on Numerical Analysis 31 (1994) 324–343.
[20] D. Kroner, S. Noelle, M. Rokyta, Convergence of higher order upwind finite volume schemes on unstructured grids for scalar conservation laws in several space dimensions, Mathematics of Computation 71 (1995) 527–560.
[21] D. Kroner, M. Ohlbefger, A posteriori error estimates for upwind finite volume schemes for nonlinear conservation laws in multi-dimensions, Numerische Mathematik 69 (2000) 25–39.
[22] M. Feistauer, J. Felcman, On the convergence of a combined finite volume-finite element for nonlinear convectioncdiffusion problems, Numerical Methods for Partial Differential Equations 13 (1997) 163–190.
[23] P. Sun, G. Xue, C. Wang, J. Xu, A domain decomposition method for two-phase transport model in the cathode of a polymer electrolyte fuel cel, Journal of Computational Physics 228 (2009) 6016–6036.
[24] C. Johnson, A. H. Schatz, L. B. Wahlbin, Crosswind smear and pointwise errors in streamline diffusion finite element methods, Mathematics of Computation 49 (1987) 25–38.
[25] T. Kang, D. Yu, Some a posteriori error estimates of the finite-difference streamlinediffusion method for convection-dominated diffusion equations, Advances in Computational Mathematics 15 (2001) 193–218.
[26] K. Niijima, Pointwise error estimates for a streamline diffusion finite element scheme, Numerische Mathematik 56 (1990) 707–719.
[27] V. John, G. Matthies, F. Schieweck, L. Tobiska, A streamline-diffusion method for nonconforming finite element approximations applied to convection-diffusion problems, Computer Methods in Applied Mechanics and Engineering 160 (1998) 85–97.